JOURNAL OF BIOMOLECULAR STRUCTURE AND DYNAMICS
https://doi.org/10.1080/07391102.2020.1868337



# Molecular mechanism of inhibition of COVID-19 main protease by β-adrenoceptor agonists and adenosine deaminase inhibitors using *in silico* methods

Pushyaraga P. Venugopal and Debashree Chakraborty

Biophysical and Computational Chemistry Laboratory, Department of Chemistry, National Institute of Technology Karnataka, Mangalore, India

Communicated by Ramaswamy H. Sarma

**ABSTRACT**

Novel coronavirus (COVID-19) responsible for viral pneumonia which emerged in late 2019 has badly affected the world. No clinically proven drugs are available yet as the targeted therapeutic agents for the treatment of this disease. The viral main protease which helps in replication and transcription inside the host can be an effective drug target. In the present study, we aimed to discover the potential of β-adrenoceptor agonists and adenosine deaminase inhibitors which are used in asthma and cancer/inflammatory disorders, respectively, as repurposing drugs against protease inhibitor by ligand-based and structure-based virtual screening using COVID-19 protease-N3 complex. The AARRR pharmacophore model was used to screen a set of 22,621 molecules to obtain hits, which were subjected to high-throughput virtual screening. Extra precision docking identified four top-scored molecules such as +/−-fenoterol, FR236913 and FR230513 with lower binding energy from both categories. Docking identified three major hydrogen bonds with Gly143, Glu166 and Gln189 residues. 100 ns MD simulation was performed for four top-scored molecules to analyze the stability, molecular mechanism and energy requirements. MM/PBSA energy calculation suggested that van der Waals and electrostatic energy components are the main reasons for the stability of complexes. Water-mediated hydrogen bonds between protein-ligand and flexibility of the ligand are found to be responsible for providing extra stability to the complexes. The insights gained from this combinatorial approach can be used to design more potent and bio-available protease inhibitors against novel coronavirus.

**ARTICLE HISTORY**
Received 1 September 2020
Accepted 17 December 2020

**KEYWORDS**
Coronavirus main protease; repurposing of drug; β-adrenoceptor agonists; adenosine deaminase inhibitors; molecular dynamics simulation

## Introduction

The current global pandemic of COVID-19 has affected more than 213 countries since its emergence in late 2019. This respiratory disease is caused by novel virus strain of family *Coronaviridae*; SARS Cov-2 (nCoV) which is an enveloped, positive-sensed, single stranded RNA betacoronavirus. As of 17 November 2020, 54.8 million people have been infected and 1.3 million people have died of SARS CoV-2. The evidences suggest that nCoV has a zoonotic source similar to SARS (severe acute respiratory syndrome) coronavirus and MERS (Middle East respiratory syndrome) coronavirus (Ahmad et al., 2020). Clinically proven antiviral drugs and vaccines are not available for SARS, MERS and COVID-19 pandemic. Currently, the treatment of COVID-19 uses remdesivir (viral RNA polymerase inhibitor), hydroxychloroquine (anti malarial drug), lopinavir/ritonavir (anti HIV drugs- protease inhibitors) and dexamethasone (corticosteroid medication). Studies show that these medications showed little or no reduction in the mortality rate of hospitalized patients when compared to normal cases. Since inventing a FDA approved drug after all the clinical trials is time taking process, repurposing of already available drugs can be a better solution for the treatment of COVID-19. Therefore, to develop therapeutic strategies for COVID-19, it is necessary to understand the mechanism of action of various viral enzymes.

*Coronaviridae* have the largest positive stranded RNA genome of 26 to 32 kb among the known RNA viruses (Schoeman & Fielding, 2019). The sequence analysis of SARS Cov-2 isolates reveal that the genome encodes for 16 non-structural proteins (Nsp 1–16) which forms replicase/transcriptase complex (RTC), 4 structural proteins (spike, envelope, membrane, nucleocapsid) and 9 putative accessory factors (Fehr & Perlman, 2015; Gordon et al., 2020; Wu et al., 2020). Among these proteins, main protease ($M^{pro}$) plays a major role in the life cycle of novel coronavirus and is the key enzyme for replication and transcription process. $M^{pro}$ process the precursor polyproteins to form functional proteins inside the virus, mainly the post-translational processing of replicase polyprotein (Wang et al., 2016). Main protease is a 34 kDa protein (306 amino acid residues), which is composed of 3 domains. Domain I (8–101 residues), domain II (102–184 residues) has an antiparallel β-barrel

CONTACT Debashree Chakraborty debashree@nitk.edu.in Biophysical and Computational Chemistry Laboratory, Department of Chemistry, National Institute of Technology Karnataka, Surathkal, Mangalore, Karnataka 575025, India

Supplemental data for this article can be accessed online at https://doi.org/10.1080/07391102.2020.1868337

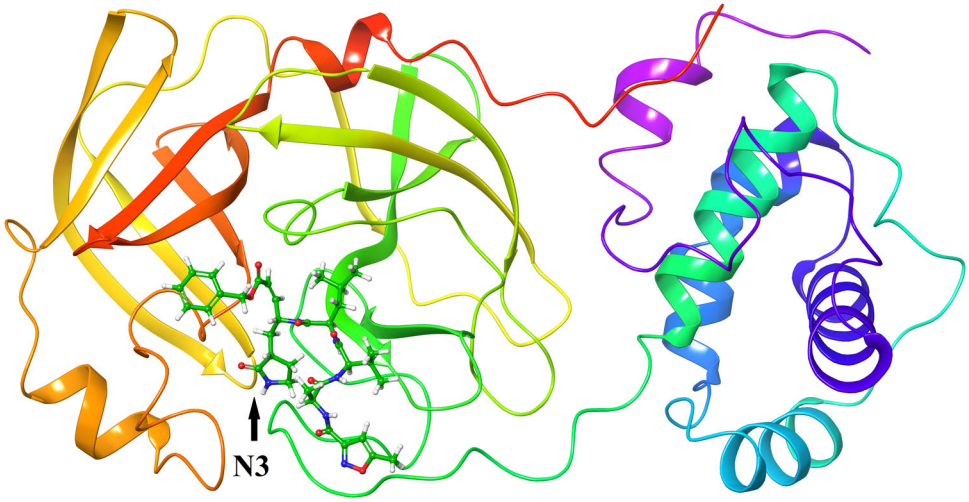


Figure 1. Crystal structure of SARS CoV-2 main protease ($M^{pro}$) complex with Michael acceptor inhibitor N3 (PDB ID: 6LU7).

structure and domain III (201–303 residues) has 5 α-helices arranged into an antiparallel globular structure. Domain III is connected to II by a loop region containing residues 185–200 (Jin et al., 2020). The substrate binding site and the Cys-His catalytic dyad are found in the cleft between domain I and domain II, similar to previously reported coronavirus protease (Ren et al., 2017; Xue et al., 2008; Yang et al., 2003). The activity of protease is triggered by the binding of small organic molecules to the substrate binding site of the enzyme. However, this process can be blocked by inhibitors, which binds to the active site, thereby inhibiting the action of enzyme. The inhibition of main protease enzyme blocks the vital polyprotein processing in coronavirus. Recent literatures suggest that small organic molecules such as polyphenols, alkamides, piperamides can effectively inhibit protease enzyme which can be developed as effective therapeutic drugs (Bolelli et al., 2020; Chojnacka et al., 2020; Gutierrez-Villagomez et al., 2020; Jin et al., 2020; Kumar, Singh, et al. 2020; Kumar, Kumari, et al., 2020; Narkhede et al., 2020). Also, repurposing of existing drugs helps us to understand the probable essential molecular structure of the drugs which can be used for the inhibition of the protease (Baby et al., 2020; Riva et al., 2020; Shah et al., 2020; Zhou et al., 2020). Therefore, $M^{pro}$ is an ideal and attractive target for the design and development of effective drug candidates against SARS CoV-2.

Thus, the objective of the present study is to understand the molecular mechanism of main protease inhibition by potential drug candidates using virtual screening (VS) and molecular dynamics (MD) simulations. Preference was given to the existing drug molecules such as β-adrenoceptor agonists and adenosine deaminase inhibitors which can be used as repurposing drug against $M^{pro}$ inhibitors since β-adrenoceptor agonists are used in the treatment of bronchial asthma (Barisione et al., 2010) whereas adenosine deaminase inhibitors are used in the treatment of cancer and inflammatory disorders (Glazer, 1980; Trincavelli, 2013). The identification of lead molecules was done by both ligand-based and structure-based virtual screening methods. The crystal structure of $M^{pro}$ complex with Michael acceptor inhibitor N3 (Jin et al., 2020) was used as the template for virtual screening methods (Figure 1). The pharmacokinetic profiles of the top-scored molecules were analyzed by ADME/Toxicity analysis. MD simulations were performed to observe the protein-ligand interactions and the stability of the complex formed by top-scored ligands. This was followed by free energy calculation by MM/PBSA (molecular-mechanics Poisson-Boltzmann surface area) method to understand the energy requirements for stable ligand-binding at the active site. Further, principal component analysis (PCA) and FEL (free energy landscape) analysis were carried out to understand the conformational changes in protease on ligand binding and the thermodynamic stability of complex.

This work is of the first kind where β-adrenoceptor agonists and adenosine deaminase inhibitors are proposed as effective inhibitors of SARS CoV-2 main protease ($M^{pro}$). Also, this work analyzes the detailed molecular mechanism and energy requirements for the ligand to act as effective protease inhibitors. Repurposing of existing drug molecules helps us to reduce the time required to develop new molecules as an effective inhibitor. The insights obtained from this study can be used to design new drug molecules with higher biological activity to treat COVID-19. The manuscript is arranged as follows. The methodology of VS and simulation details were given in Methods section. Results and Discussion section includes the results obtained from VS, MD simulation, PCA, FEL analysis and binding free energy analysis. Conclusion includes the major outcomes obtained from this study.

## Materials and methods

### *Ligand selection*

The three-dimensional structures of the drug candidates were retrieved from ZINC database based on the Lipinski's rule (Irwin et al., 2012). Approximately, 22621 molecules were obtained from the ZINC database for ligand-based virtual screening. LigPrep module (Schrödinger 2020-1) was used to prepare the ligands. The low energy conformations of the ligand with possible ionization states were generated

at pH value 6.0. A total of 45907 conformations were generated from the dataset after adding hydrogen and removing small fragments. Further, the geometry of resultant drug candidates was refined by LigPrep module using OPLS_2005 force field (Jorgensen et al., 1996; Kaminski et al., 2001).

### Pharmacophore model generation

The crystal structure of COVID-19 main protease with Michael acceptor inhibitor N3 (PDB ID: 6LU7, resolution: 2.16 Å) (Jin et al., 2020) was used as initial structure for pharmacophore modeling. N3 was developed using computational drug-designing sources and found to inhibit protease effectively with $K_{obs}/[I]$ value of $11300 \pm 880\ M^{-1}s^{-1}$ equivalent to dissociation constant (Jin et al., 2020). The protein was prepared at an experimental pH of 6.0 using PROPKA program and Phase module (Schrödinger 2020-1) was used to generate the pharmacophore model based on the protein-ligand interactions using 'Receptor-ligand complex' option. The pharmacophore model was developed with hydrogen bond acceptors (A) and aromatic rings (R). Pharmacophore-based screening was done with the prepared ligands from ZINC database. Minimum matches of 4 out of 5 sites were set as the criteria to obtain ligands with desired features. The final hits were ranked according to the Phase fitness score, align score, vector score and volume score (Dixon et al., 2006).

### Molecular docking-based screening

Ligand-based virtual screening by pharmacophore model identified 5297 hits from ZINC database based on the fitness score. Since the database is larger for molecular docking, the ligands were subjected to high-throughput virtual screening (HTVS). All molecular docking studies were carried out using Glide module (Schrödinger 2020-1). Docking based screening is done by three steps, HTVS, standard precision (SP) and extra precision (XP). Five hundred and twenty-nine compounds from ZINC database were used for further screening using SP mode of molecular docking. Out of these compounds, 52 compounds from the database were selected for XP mode of docking. Finally, two top-scored ligands each from both categories were chosen for post dock analysis. For comparison, two other crystal structures of main protease with a broad spectrum non-covalent inhibitor X77 (6W63) and alpha-ketoamide 13 b (6Y2G) and Apo $M^{Pro}$ (7KFI) were used for better insight of the ligand binding site of the enzyme (Figure S1).

### ADME/toxicity studies

The drug-likeness of a molecule can be predicted by pharmacokinetic (PK) properties. The ADME/Tox profile and molecular descriptors of the top-scored hits were predicted by Qikprop module (Schrödinger Release 2020-1). The properties like absorption, distribution, metabolism, excretion and toxicity (ADMET) were determined in order to confirm the effectiveness and bioavailability of predicted molecules in accordance with Lipinski's rule (Lipinski, 2004). The molecular weight (MW), number of hydrogen bond donor-acceptor groups and octanol/water partition co-efficient ($P_{o/w}$) of top-scored β-adrenoceptor agonists and adenosine deaminase inhibitors are evaluated based on rule of five to predict their drug-likeness.

### MD simulation protocol

MD simulation is an important tool to understand the structural and dynamical behavior of biological system (Daddam et al., 2020; Das et al., 2019; Venugopal et al., 2020). The stability of complex formed between covid-19 main protease (6LU7) and the top-scored ligands was analyzed by 100 ns simulations by Gromacs 2018.4 (Abraham et al., 2015) using SPC/E water model (Mark & Nilsson, 2001). The protein topology was generated using AMBER99SB force field (Hornak et al., 2006). The complex was solvated in a cubic box with 1 nm edges and neutralized with $Na^+$ ions. The energy minimization of system was done by steepest descent algorithm with a maximum of 50000 steps until a convergence tolerance of 10 $kJmol^{-1}$. A 10 ns NVT and NPT equilibration were carried out at 300 K and 1.0 atm, respectively, throughout the process (Bussi et al., 2007; Martyna et al., 1992; Parrinello & Rahman, 1981). Lastly, a 100 ns production run was performed by removing restrain to relax the protein-ligand system and trajectories were saved at every 10 ps for analysis. Three independent simulations (a total of 12 simulations) were performed for each protein-ligand system to check the reproducibility of the results. A 100 ns simulation for $M^{Pro}$/N3 (6LU7), $M^{Pro}$/X77 (6W63) and $M^{Pro}$/13b (6Y2G) complexes was also performed to analyze the stability of native inhibitor N3 and to compare the efficiency of predicted inhibitors. To quantify the binding free energy, MM/PBSA energy calculations were done by g_mmpbsa tool (Open Source Drug Discovery Consortium, 2014) using MD trajectories. PCA describes the dynamics of biomolecules with reduced degrees of freedom through observed motions which spans from largest to smallest. PCA was performed for backbone atoms on 100 ns MD trajectory using Gromacs 2018.4. Using in-house scripts, the eigenvalues and corresponding eigenvectors of the system were calculated. Free energy landscapes were constructed using PC1 and PC2 to study the most stable protein-ligand binding conformational states.

## Results and discussion

### Pharmacophore-based virtual screening

Based on $M^{Pro}$ (6LU7)-imidazole carboxamide complex (receptor-ligand complex), five-featured pharmacophore model, AARRR, consisting of two hydrogen bond acceptor (A3 and A4) and three aromatic rings (R9, R10 and R11) were generated (Figure 2). The acceptor A3 lies toward Asn142, Gly143 residues and acceptor A4 lies towards Glu166, Leu167 residues. The aromatic rings R10 and R11 were found to be near to aromatic amino acid residues, i.e. Phe140, Hie163, His164 and Pro52, Tyr54, respectively. In covid-19 main

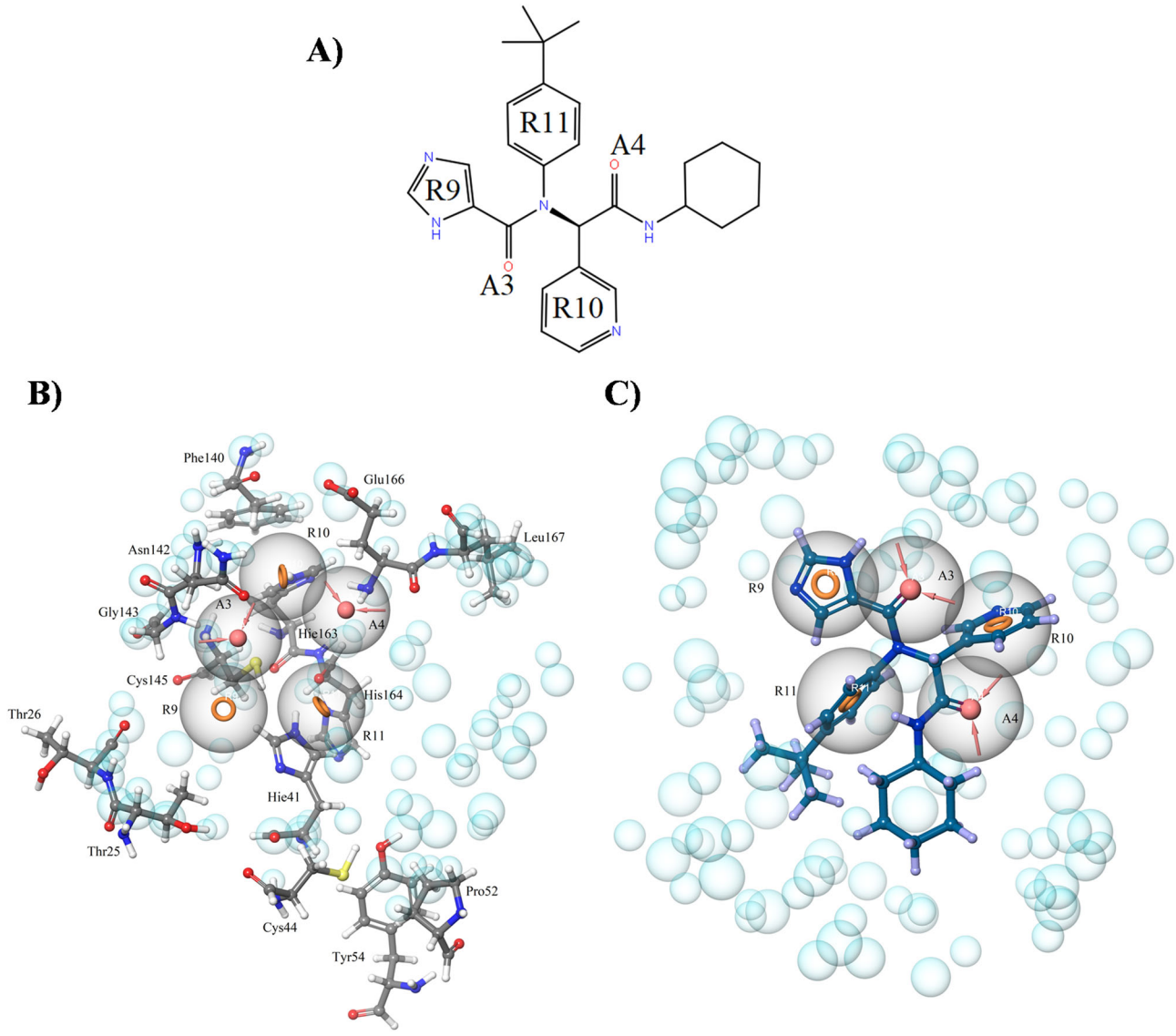


Figure 2. (A) Structure of broad spectrum non-covalent inhibitor, derivative of imidazole carboxamide. (B) Pharmacophore model (AARRR) generated using Phase module inside the binding pocket of covid-19 main protease. (C) Overlay of inhibitor over the generated model. The spheres indicate the excluded volume forbidden for ligands due to enzyme backbone or lipophilic interactions.

protease, the Nε2-protonated tautomeric form (Hie) of histidine amino acid (His) (Li & Hong, 2011) is present at the binding site. The ring R9 is found close to Thr25, Thr26 and Cys145. A dataset containing 22,621 drug-like molecules were screened using AARRR pharmacophore model as template to obtain drug candidates with similar pharmacophore. Around 5300 molecules were obtained as top hits for structure-based virtual screening.

## Molecular docking analysis

A dataset of 5300 top-selected molecules from pharmacophore-based screening were subjected to structure-based virtual screening via HTVS mode with main protease (6LU7). The van der Waals scaling factor for proteins was set to 1.0 cut-off and a grid of 72 Å dimension was generated at protease binding site. HTVS is usually employed when the database is large for molecular docking process. A total of 704 molecules obtained from HTVS, were then subjected to docking via SP mode. The number of molecules was reduced to 52, which were subjected to extra precision (XP) docking. The docking score of top-scored hit molecules ranges from −9.491 to −7.526 kcal/mol for adrenoceptor agonists and −9.155 to −8.004 kcal/mol for adenosine deaminase inhibitors (Table 1). The four top-scored molecules predicted by XP mode of molecular docking are (S,R)-(+)-fenoterol, (R,R)-(−)-fenoterol, FR236913 and FR230513. Fenoterol is β adrenoreceptor agonist which is used as asthma medication (Svedmyr, 1985). Compounds, FR236913 and FR230513, are potent adenosine deaminase inhibitors (Terasaka, Kinoshita, Kuno, & Nakanishi, 2004; Terasaka, Kinoshita, Kuno, Seki, et al., 2004). The overlay of top-scored molecules obtained from XP mode of docking over the developed pharmacophore model is shown in Figure S2. Both the inhibitor category satisfied at least three chemical features, namely the two aromatic rings and one hydrogen bond acceptor which correlate well with the developed AARRR pharmacophore model. The highest docking scored + (-) Fenoterol molecule possesses two aromatic rings which can

**Table 1.** Molecular structure, common name, docking score and 2D ligand interaction diagrams of top-scored hit molecules with main protease (6LU7).

| Structure and name<br>Docking score (kcal/mol) | 2D ligand interaction diagram |
|---|---|
| Inhibitor, N3<br>DS = −7.128 | 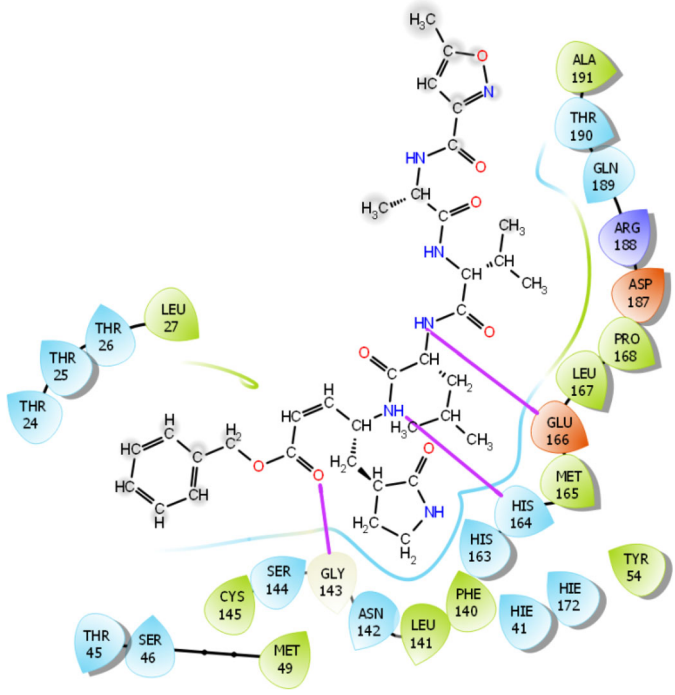 |
| **Adrenoceptor agonists**<br> 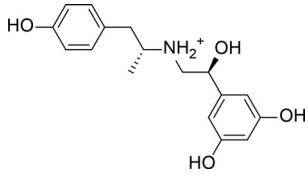 <br>(S,R)-(+)-fenoterol<br>DS = −9.491 | 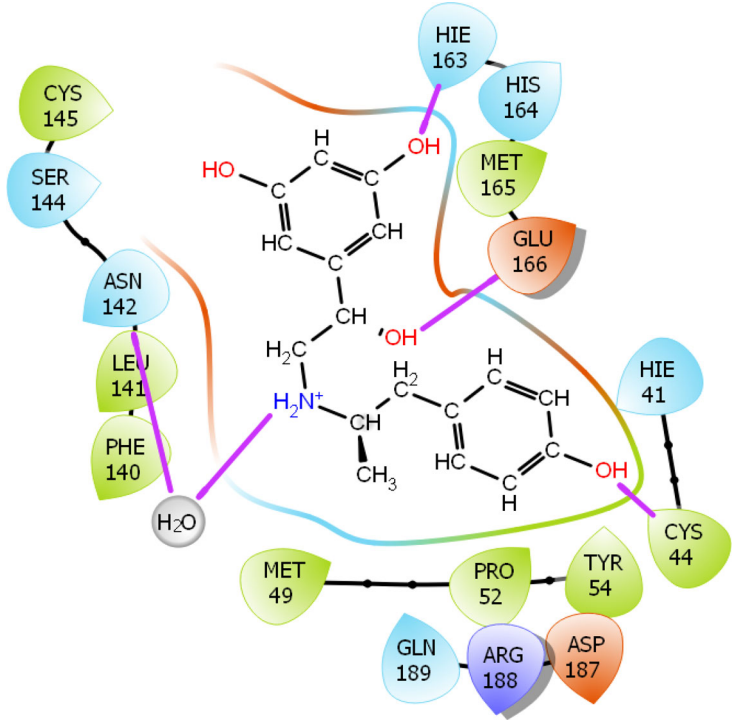 |

(*continued*)

hold the ligand at protein catalytic site by stacking interactions. The molecule has two sets of oxygen atoms which can act as hydrogen bond acceptor with Glu166 (H) and Gly143 (H). In case of adenosine deaminase inhibitors (FR236913 and FR230513) two aromatic rings are found in the structure which contributes to the activity but at slightly different sites compared to the developed model. FR236913 molecule has one acceptor carbonyl oxygen which interacts with Gln189 (H); whereas FR230513 has two hydrogen bond acceptor groups. The nitrogen atom present at the indole ring of the inhibitor interacts with Glu166 (H) and the carbonyl oxygen of the inhibitor was found to form random hydrogen bonds with

Table 1. Continued.

| Structure and name<br>Docking score (kcal/mol) | 2D ligand interaction diagram |
|---|---|
| 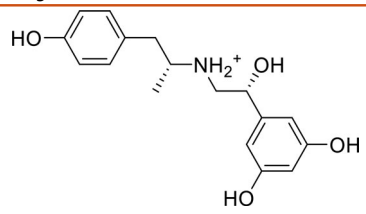 <br>(R,R)-(−)-fenoterol<br>DS = −9.425 | 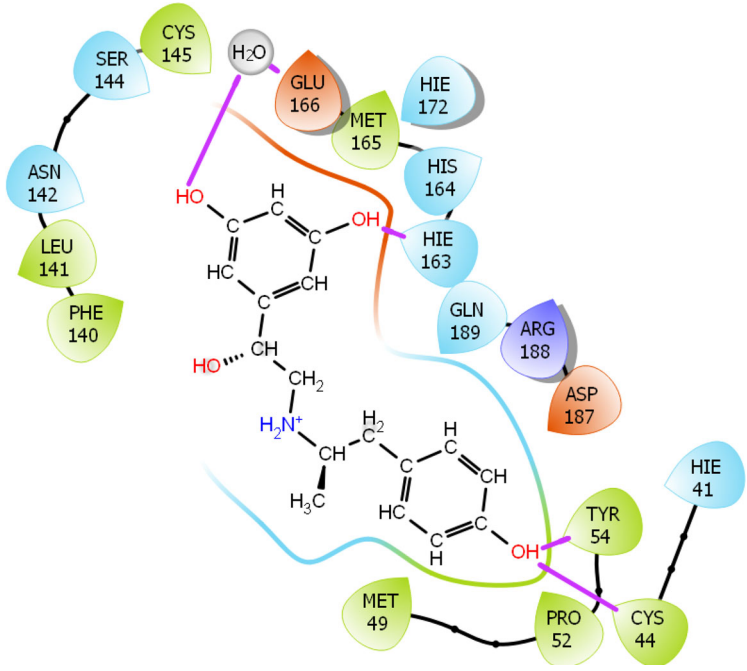 |
| 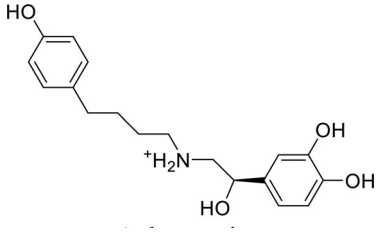 <br>Arbutamine<br>DS = −8.195 | 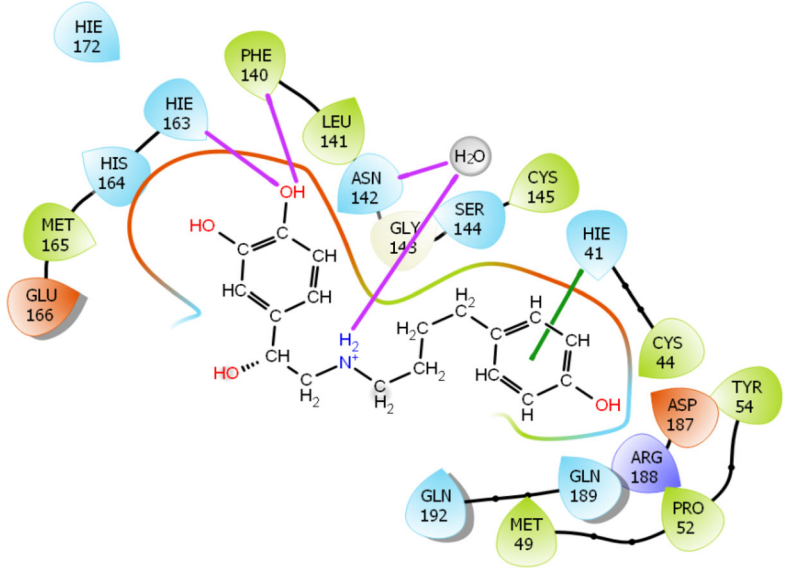 |

(*continued*)

Gly143, Ser144 and Cys145. Thus aromatic rings and hydrogen bond donor-acceptor groups are important chemical features for the inhibitors as obtained by the developed pharmacophore model.

2D Ligand interaction diagram (Table 1) showed the possibilities of hydrogen bonding between acceptor site of ligand and amino acid residues such as Glu166, Gln189, Gly143, Phe140 and Hie163 of covid-19 main protease. Also, there is lesser possibility of hydrogen bond formation with the residues Cys44, Cys145 and π-stacking interaction with the residue Hie41. It is found that the complex is stabilized by hydrophobic interaction as well as polar interaction. The presence of water mediated hydrogen bonds further increase the stability of the complex. The protonated form of compound, (S,R)-(+)-fenoterol showed the highest docking score (−9.491) and found to have hydrogen bonding interaction with Cys44, Hie163 and Glu166. This compound also showed a water-mediated hydrogen bond with Asn142. The second potent ligand with lowest binding energy (−55.55 kcal/mol) is showed by (R,R)-(−)-fenoterol which is a conformer of fenoterol. From docking studies, it is found that both the enantiomers of fenoterol are found to be potent inhibitors against protease enzyme among adrenoceptor agonists. Similarly, among adenosine deaminase inhibitors, FR236913 and FR230513 are found to be potent ligands against protease. The compound, FR236913 showed hydrogen bonding

Table 1. Continued.

| Structure and name<br>Docking score (kcal/mol) | 2D ligand interaction diagram |
|---|---|
| 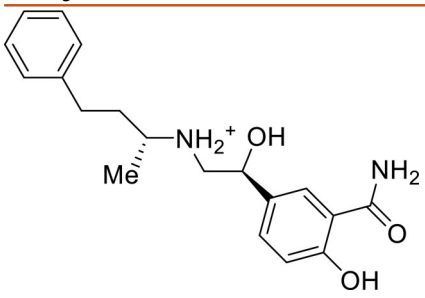 <br>Ractopamine hydrochloride<br>DS = −7.526 | 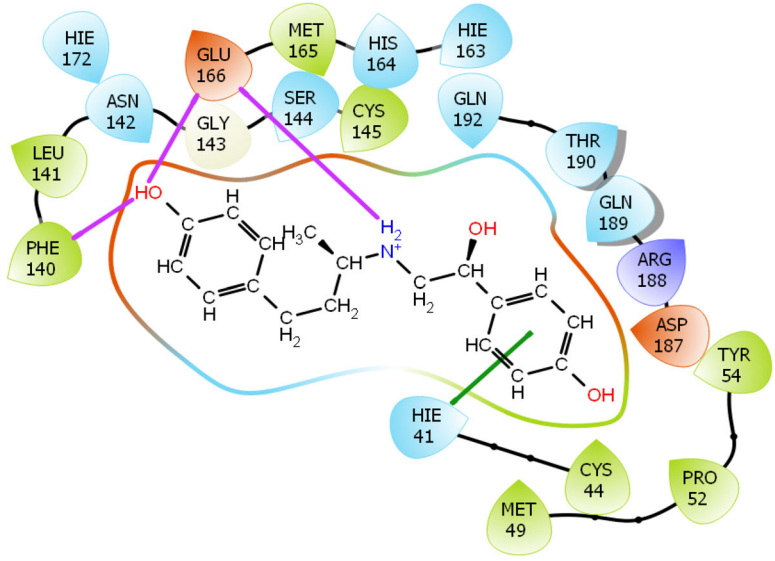 |
| **Adenosine deaminase inhibitors**<br> 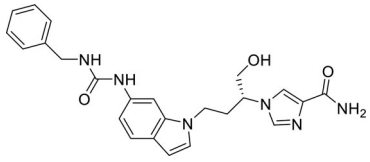 <br>FR236913<br>DS = −9.163 | 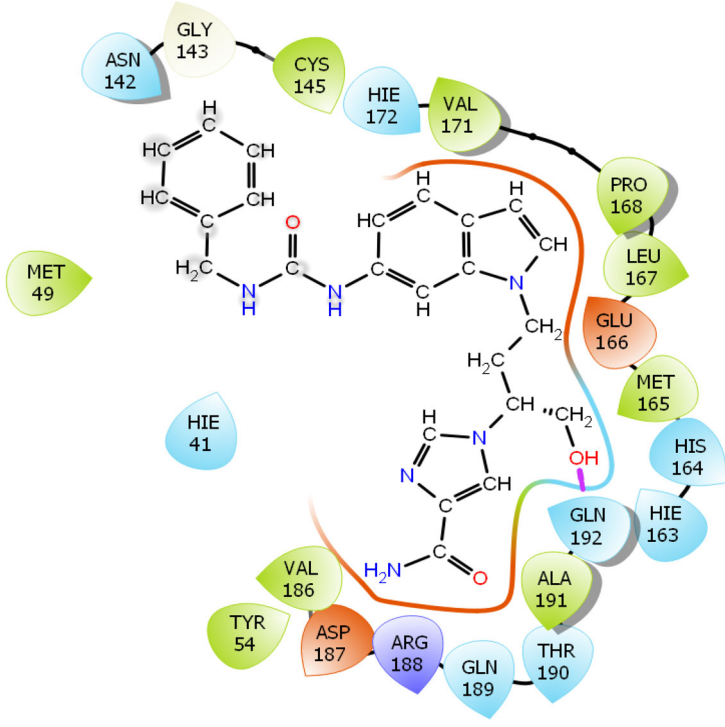 |

(*continued*)

interaction with Phe140, Gly143, Hie163 and Gln189. Additionally, it showed stacking interaction with Hie41. The compound, FR230513 showed only three hydrogen bonds with residues Phe140, Gly143 and Hie163. Apart from hydrogen bonds, all the complexes are stabilized by hydrophobic interactions and polar interactions.

The top-scored molecules were docked to other crystal structures of main protease (6Y2G and 6W63) and apo form (7KFI) for comparison. The docking score and interactions of native inhibitors of main protease are given in Table S1. The interactions of ligands with the amino acid residues at binding sites of 6Y2G, 6W63 and apo form are found to be similar to 6LU7 structure. Mainly, the molecules form hydrogen bond interaction with Gly143, Hie163 and Glu166. The docking score suggests that the screening results of 6LU7 are well correlated with other crystal structures of main protease (Table S2).

## *ADME/toxicity prediction of top-scored hits*

The ADME/Toxicity values for the top-scored hits are given in Table S3. The molecules are evaluated by Lipinski's rule of five and percent of human oral absorption. The values are

Table 1. Continued.

| Structure and name<br>Docking score (kcal/mol) | 2D ligand interaction diagram |
|---|---|
| 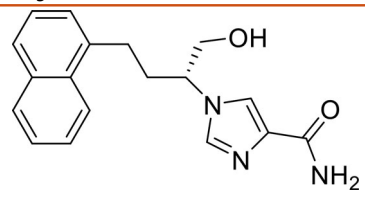 <br>FR230513<br>DS = −9.049 | 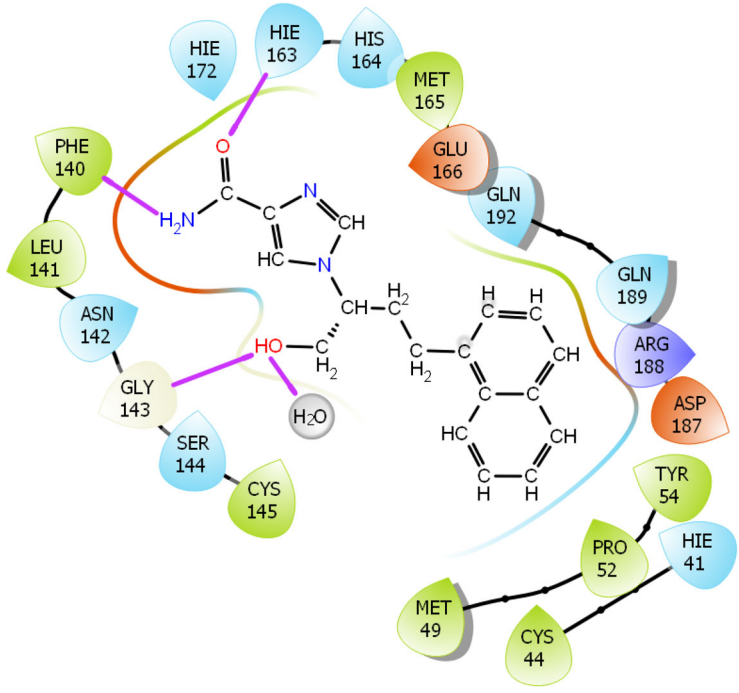 |
| 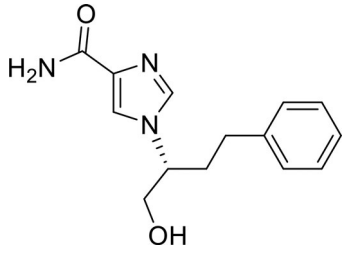 <br>FR221647<br>DS = −8.221 | 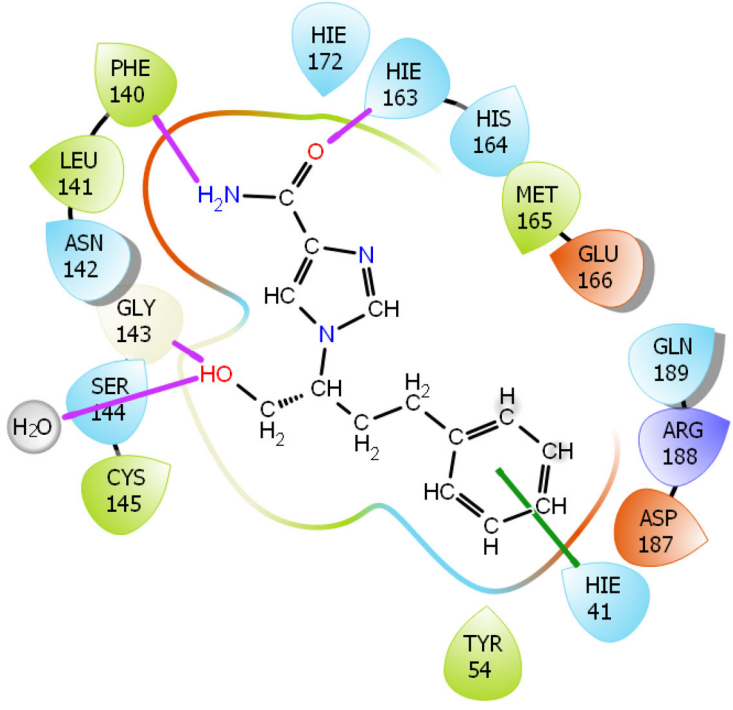 |

(*continued*)

found to be in permissible limit for bioavailable drugs (Table S3). All the top-scored hits obeyed Lipinski's rule of five. The percentage of human oral absorption values are found to be in the permissible range (> 80% high and < 25% poor). All the top-scored molecules found to have molecular weight, solvent accessible surface area (SASA), hydrogen bond acceptor-donor groups, octanol/water partition coefficient (QPlogPo/w), polar surface area (PSA) and solubility (QPlogS) in acceptable range. The compound, +/−-Fenoterol found to follow the acceptable range of ADMET properties and obeys Lipinski's rule of 5. In the case of FR236913, it is found that dipole moment is 12.06 debye, predicted blood/brain partition coefficient (QPlogBB) is −2.898, SASA is 817.883 Å$^2$, solubility is −5.312, predicted percent of oral absorption is 80.010% and PSA is 138.831 Å$^2$ which are toward the upper limit of acceptable range.

Table 1. Continued.

| Structure and name<br>Docking score (kcal/mol) | 2D ligand interaction diagram |
|---|---|
| 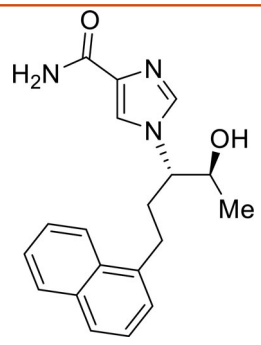 <br>FR233623<br>DS = −8.004 | 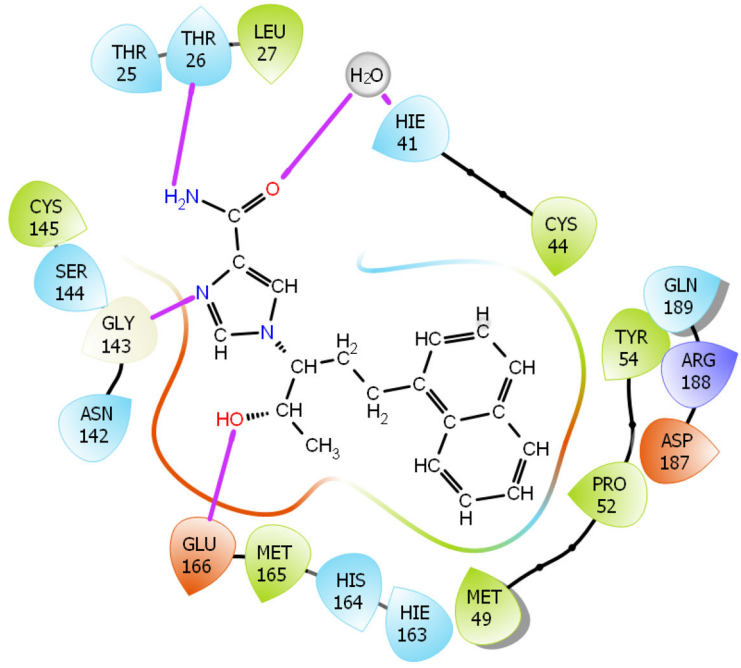 |



*LID Legend.


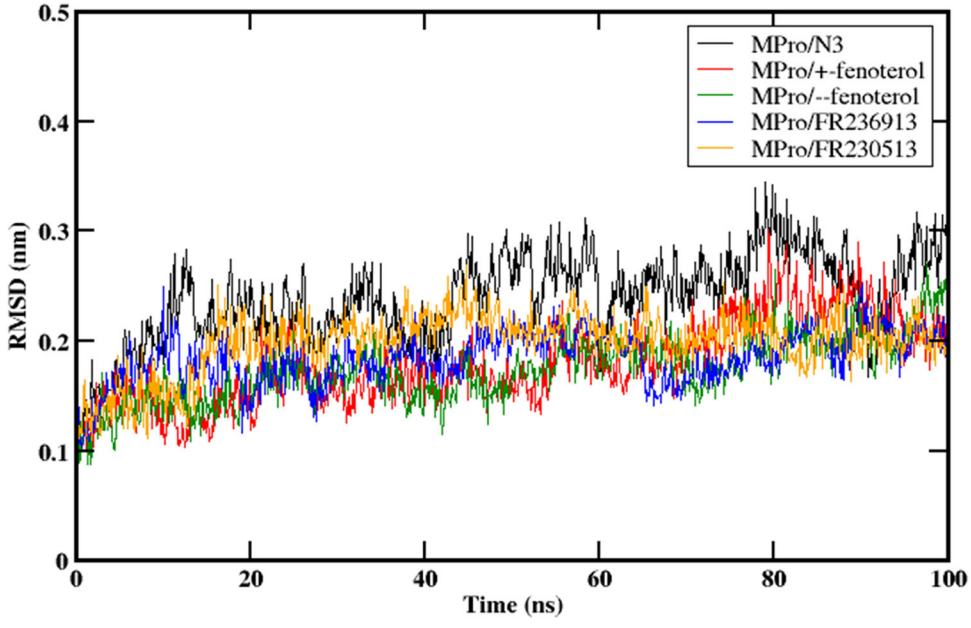


Figure 3. RMSD profile of backbone of covid-19 main protease (6LU7) complexed with Michael acceptor inhibitor N3 and top-scored hits over 100 ns trajectory.

## *Molecular dynamics simulation*

Three independent 100 ns MD simulation (a total of 12 simulations) was performed for the inhibitor complexes of four top-scored hits with main protease (6LU7) to analyze the stability, molecular mechanism and energy criteria. Further, three more 100 ns simulation of main protease with N3 and 13 b (co-crystal inhibitors) were performed to compare the

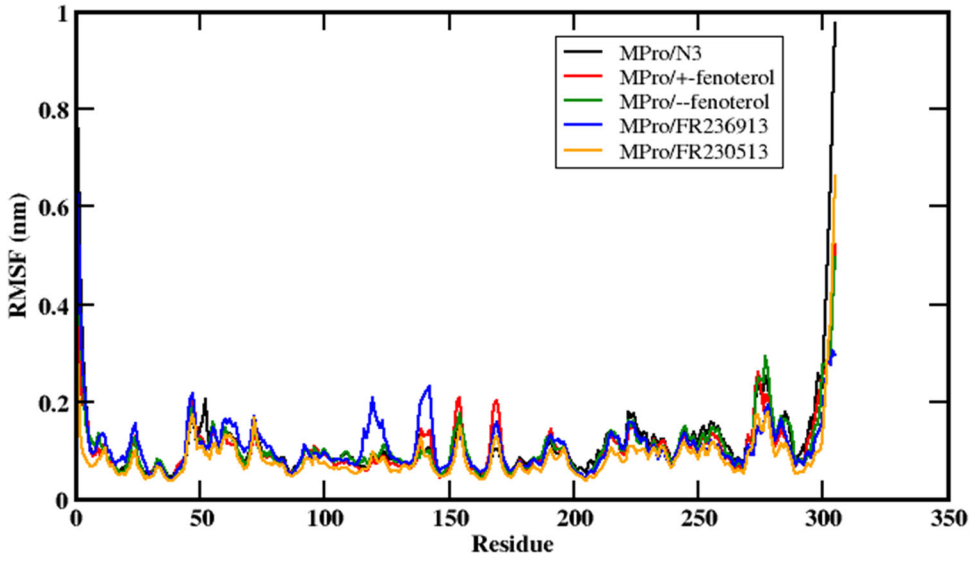


Figure 4. Residue-based fluctuations of protease (6LU7) backbone of complexes over 100 ns simulation.

efficiency of predicted molecules and results of 6Y2G/13b complex are given in Figure S3.

### Stability of protein-ligand complex

The backbone RMSD (root mean square deviation) profile for main protease complexes are shown in Figure 3. The RMSD profile suggested that the complexes are stabilized after 25 ns of simulation. The average RMSD value for the complex of Michael acceptor N3 is found to be 0.24 nm. The average RMSD values for the backbone atoms of complex of +-fenoterol, −-fenoterol, FR236913 and FR230513 for three independent simulations are found to be 0.193 ± 0.014 nm, 0.179 ± 0.008 nm, 0.202 ± 0.021 nm and 0.193 ± 0.012 nm, respectively. It is evident from the RMSD profile that the complexes of top-scored hits are stable than the co-crystal inhibitor N3. The detailed analysis of each simulation is given in Table S4. To check for the convergence, RMSD block averaging has been performed by taking 10 ns fragments of last 50 ns MD trajectory (Table S5). The standard deviation of each block is in range 0.01–0.02 which indicates less fluctuation and convergence of data.

RMSF (Root Mean Square Fluctuation) profile describes the behavior of movements of amino acid residues. Lower value of RMSF indicates rigid structure while higher value indicates loosely bounded structure. The average RMSF value of main protease bound to Michael acceptor N3, +-fenoterol, −-fenoterol, FR236913 and FR230513 are found to be 0.116 nm, 0.103 nm, 0.107 nm, 0.109 nm and 0.086 nm, respectively (Figure 4). The region from Thr25- Arg60 and Thr135- Ile200 which showed interaction with the ligand has lower fluctuations than in the complex of N3, +/−-fenoterol and FR230513. The RMSF values of these residues lies in the range of 0.07- 0.09 nm. MPro/+-fenoterol complex is found to be more stable with fewer fluctuations. The complex MPro/FR236913 showed an opposite trend with higher fluctuations at this region.

The compactness of protease inhibitor complexes were predicted by rGyr (radius of gyration) values throughout the 100 ns simulation. The Rg plots are shown in Figure 5 and the average rGyr values for +-fenoterol, −-fenoterol, FR236913 and FR230513 complexes are found to be 2.198 ± 0.009 nm, 2.198 ± 0.016 nm, 2.191 ± 0.013 nm and 2.207 ± 0.017 nm, respectively. The Rg value for N3 is found to be 2.218 nm. From the Rg values, it is clear that all the inhibitor complexes are compact and stable compared to the native inhibitor N3.

The main protease bound to inhibitor 13 b (6Y2G) found to have higher RMSD value, higher RMSF fluctuations and lower compactness (higher Rg value) compared to above discussed complexes (Mittal et al., 2020) (Figure S3).

### Secondary structure analysis

Per-residue secondary structure analysis of the protein suggests that there are no considerable changes in the structure of enzyme on inhibitor binding (Figure S4). The average occupancy of secondary structure components such as β-sheet, β-bridge, α-helix, bend, coil, 5-helix and 3-helix are shown in Figure 6. There is an insignificant presence of 5-helix in +/− fenoterol, FR236913 complexes during the course of simulation while 5-helix is absent in FR230513 complex. α-helix which found to be fluctuating at the initial time scale of simulation, stabilizes after 40 ns for all the complexes. β-sheets and β-bridges are found to be stable throughout the course of simulation. The secondary structure analysis suggests that there is no significant structural change at the binding site of protein on ligand binding.

### Hydrogen bonding interactions

Hydrogen bonding interactions are crucial for stable ligand binding at the binding site of protein. The average number of hydrogen bonds between protein-ligand, ligand-water and binding site residues-water are illustrated in Figure 7. Apart from the hydrogen bonds between protein and ligand,

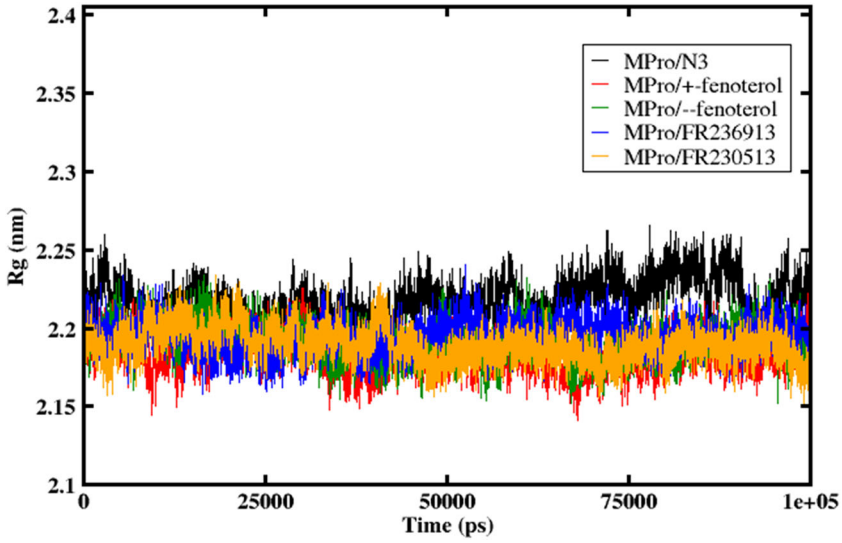


Figure 5. The plot of radius of gyration (Rg) vs. Time (ps) for Cov-2 main protease (6LU7)/inhibitor complexes.

water-mediated hydrogen bonds provide extra stability to the protein-ligand system. Hydrogen bonding interaction of ligand with Gly143, Hie163 and Glu166 residues are common in complexes (Table 2). Apart from these interactions, co-crystal inhibitor found to have interactions with His41 with 64.3% occupancy. Compound +-fenoterol forms two extra hydrogen bonds with Phe140 and Asp187 with occupancy of 18% and 22.9%, respectively, whereas –fenoterol shows three extra hydrogen bonds with Asn142 (13.4%), Asp187 (76.6%) and Cys145 (32.5%). The compound, FR236913 showed least occupancy values for all the hydrogen bonds whereas the compound, FR230513 showed major hydrogen bond occupancy with residues Glu166 (85.4%), Cys145 (59.8%) and Ser144 (41.4%). Even though similar hydrogen bond interactions are observed for all the complexes, difference in the value of hydrogen bond occupancy maybe attributed due to the possibility of acquiring various conformations during the course of simulation.

Figure 7(A) represents the hydrogen bond distribution of Michael acceptor inhibitor N3 with protein and water. It can be seen from Figure 7(B,C) that average number of hydrogen bonds formed between protein and ligand is three. Water plays an important role in stabilizing these complexes by forming hydrogen bonds with protein binding site as well as the ligands. From Figure 7(D), it is found that the average number of protein-ligand hydrogen bonds is two and the ligand is solvated more by ligand-water hydrogen bonds. Also, it can be seen in Figure 7(E) that the ligand does not form stable hydrogen bonds with protein and the ligand is solvated by water molecules. Both the ligand (FR236913 and FR230513) forms a very few water-mediated hydrogen bonds and the binding site have lesser water molecules. Therefore, hydrogen bond stabilization is seen maximum in case of +/−-Fenoterol complexes as compared to other complexes.

The hydrogen bond occupancy of MPro/X77 (6W63) and MPro/13b (6Y2G) is given in Table S6. The majority of the hydrogen bond interaction is observed with amino acid residues Glu166 (> 90%) and Gly143.

## PCA and FEL analysis

Principal component analysis (PCA) was applied on backbone atoms for a stable trajectory of 40 ns for all the complexes of protease (6LU7) to analyze the essential dynamics which governs the conformational changes during simulation. The eigenvalue rapidly decreased along the eigenvector index indicating that first three eigenvector contribute significantly to the conformational changes in the protease enzyme during the simulation (Figure 8). The first ten eigenvectors accounts for 80.71%, 70.97%, 72.54%, 66.05% and 73.43% motions for MPro/N3, MPro/+-fenoterol, MPro/−-fenoterol, MPro/FR236913 and MPro/FR230513 complexes, respectively, indicating that ligand induces conformational changes to protein on binding. PCA analysis suggests that complex of top-scored molecules are more stable than the complex of native inhibitor N3 bound to protease enzyme. PCA analysis also suggests that the compound, FR236913 binds intact to the binding site of enzyme with lowest correlated motions with the residues.

Gibbs free energy plots were constructed with PC1 and PC2 as reaction coordinates to relate the obtained structural properties with the thermodynamic information (Figure 9). The energy minima on plots indicate the stable ligand conformation at the binding pocket of enzyme over estimated time scale. The FEL of the complexes of +-fenoterol and −-fenoterol with the enzyme suggests that the ligand form a stable complex with the protein. The complex can span from one conformation to another easily with the help of interactions such as hydrogen bonds. Thus the flexibility of ligands to form hydrogen bonds with residues as well as water results in stable complex. The complexes of native inhibitor N3 and the other ligands such as FR236913, FR230513 have two well-defined regions separated by energy barriers. This is due to the reduced number of water-mediated hydrogen bonds in the complexes. The hydrogen bond distribution for FR236913 and FR230513 with the enzyme is similar which reflected in the FEL. The solvation of ligands reduces the

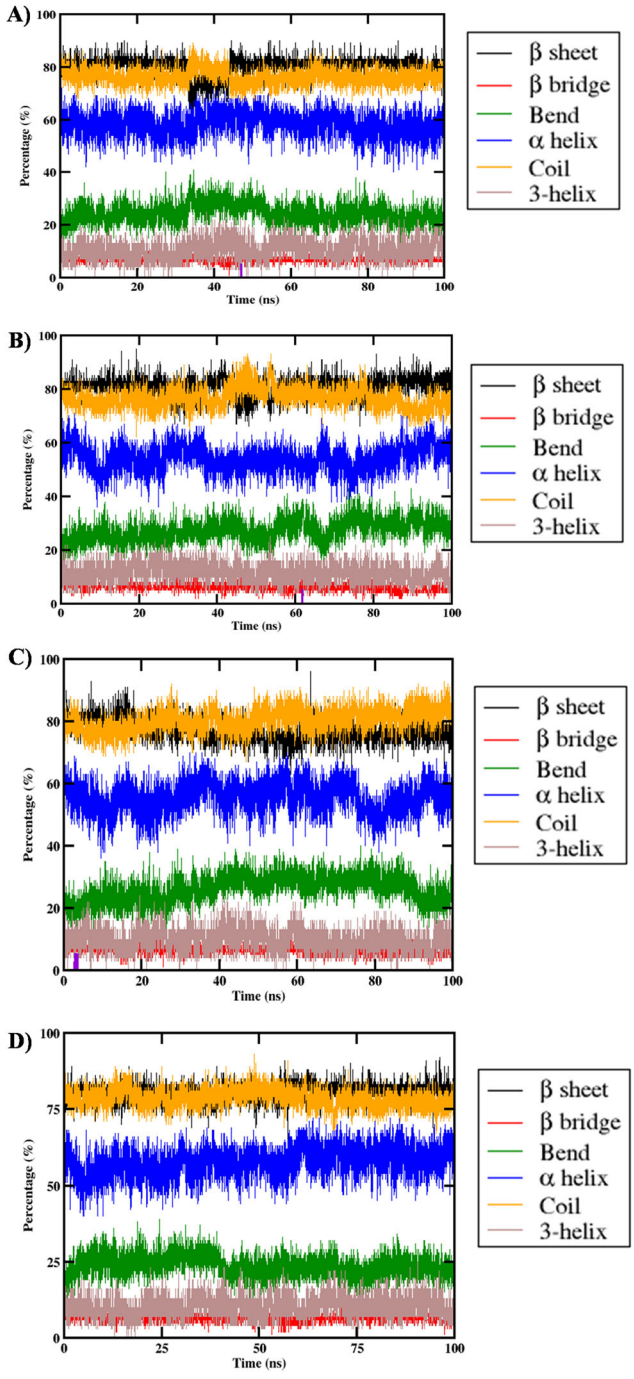


Figure 6. Occupancy of secondary structure elements of covid-19 main protease (6LU7) in the inhibitor complex. (A) MPro/+-fenoterol, (B) MPro/−-fenoterol, (C) MPro/FR236913 and (D) MPro/FR230513.

possibility of change in conformations of the complex, making separate regions for ligand-water and protein-ligand interactions.

## MM/PBSA free energy

To estimate the strength of protein-ligand interactions, binding energy analysis was carried out by MM/PBSA method for the last 75 ns of MD trajectory. The binding free energy of MPro/+-fenoterol and MPro/−-fenoterol are −217.785 and −197.351 kJ/mol, respectively, which indicates that the

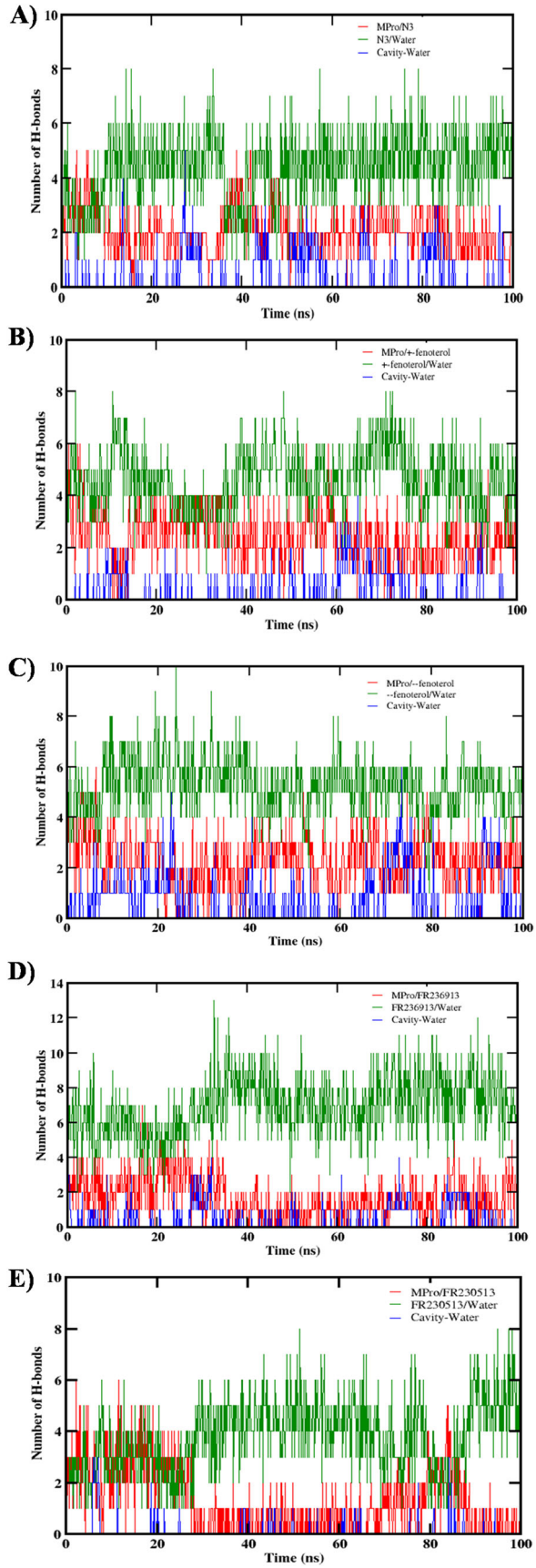


Figure 7. Hydrogen bond interactions between protease (6LU7) -inhibitor (red), inhibitor-water (blue) and binding site residues of protease-water (green). (A) MPro/N3, (B) MPro/+-fenoterol, (C) MPro/−-fenoterol, (D) MPro/FR236913 and (E) MPro/FR230513.

complexes are stable when compared to MPro/N3 (−138.788 kJ/mol), MPro/X77 (−101.042 kJ/mol) and MPro/13b (−116.501 kJ/mol). MPro/FR230513 and MPro/FR236913 has showed a stable binding free energy of −86.782 kJ/mol and −82.449 kJ/mol, respectively (Table 3). The most important contribution to the overall binding free energy is from van der Waals energy and electrostatic energy. Electrostatic contribution arises from the hydrogen bonding interactions directly from the ligands or due to the presence of water-mediated hydrogen bonds. For +/−-fenoterol the electrostatic contribution is found to be higher due to the presence of higher number of hydrogen bonds between protein and ligand. For all complexes, the contribution from van der Waals energy is quite significant which indicates the importance of hydrophobic interaction. SASA energy has a positive effect on overall energy. Lesser contribution of electrostatic energy in FR236913 and FR230513 complexes result in decrease in the binding energy compared to fenoterol complexes. It can be seen that the average number of hydrogen bonds formed between MPro/ligand and cavity/water are reduced in case of MPro/FR236913 and MPro/FR230513 complexes. The high positive value of polar solvation energy and lower contribution of electrostatic energy disfavors the ligand binding at protease enzyme which is evident from the free energy of FR236913 and FR230513 complexes. The positive value for polar energy is due to the solvation of ligand by the water molecules, thereby reducing its interaction with the protein. MM/PBSA binding free energy values of complexes of N3, FR236913 and FR230513 suggests that FR236913 and FR230513 have similar effect on protease enzyme as its native inhibitor N3. Similarly, FEL and free energy analysis suggests that +/−-fenoterol can be an effective inhibitor against protease enzyme. It is found that the adrenoceptor inhibitors shows more stable binding energy that the adenosine deaminase inhibitors. MM/PBSA energy components explain the importance of aromatic rings, hydrophobic core and hydrogen bond donor-acceptor groups in ligands as well as at the binding site. The binding free energy obtained from other two independent simulation shows good correlation and is given in Table S7.

Table 2. Hydrogen bond occupancy between ligand and residues at binding site of protease.

| System (6LU7) | Hydrogen bond occupancy (%) Donor — Acceptor | |
|---|---|---|
| MPro/N3 | N3 (H) — His41 (N) | 65.9 |
| | N3 (H) — Glu166 (O) | 93.8 |
| | N3 (H) — Thr190 (O) | 74.2 |
| | Gln189 (H) — N3 (O) | 49.2 |
| | Glu166 (H) — N3 (O) | 17.8 |
| MPro/+-fenoterol | Lig (H) — Glu166 (O) | 27.1 |
| | Lig (H) — Glu166 (O) | 33.8 |
| | Lig (H) — Hie163 (N) | 10.6 |
| | Lig (H) — Phe140 (O) | 18.0 |
| | Lig (H) — Asp187 (O) | 22.9 |
| | Glu166 (H) — Lig (O) | 50.9 |
| | Gly143 (H) — Lig (O) | 16.1 |
| MPro/−-fenoterol | Lig (H) — Asn142 (O) | 13.4 |
| | Lig (H) — Glu166 (O) | 12.5 |
| | Lig (H) — Asp187 (O) | 76.6 |
| | Glu166 (H) — Lig (O) | 11.5 |
| | Hie163 (H) — Lig (O) | 19.6 |
| | Cys145 (H) — Lig (O) | 32.5 |
| | Gly143 (H) — Lig (O) | 21.1 |
| MPro/FR236913 | Lig (H) — Phe140 (O) | 10.6 |
| | Lig (H) — Cys44 (O) | 12.0 |
| | Lig (H) — Thr190 (O) | 13.1 |
| | Lig (H) — Thr190 (O) | 11.7 |
| | Gln189 (H) — Lig (O) | 14.2 |
| | Glu166 (H) — Lig (O) | 14.2 |
| | Hie163 (H) — Lig (O) | 16.6 |
| MPro/FR230513 | Lig (H) — Ser144 (O) | 41.4 |
| | Lig (H) — Leu141 (O) | 19.6 |
| | Lig (H) — Asn142 (O) | 13.9 |
| | Glu166 (H) — Lig (N) | 85.4 |
| | Cys145 (H) — Lig (O) | 59.8 |
| | Ser144 (H) — Lig (O) | 35.0 |
| | Gly143 (H) — Lig (O) | 38.3 |
| | Asn142 (H) — Lig (O) | 25.2 |

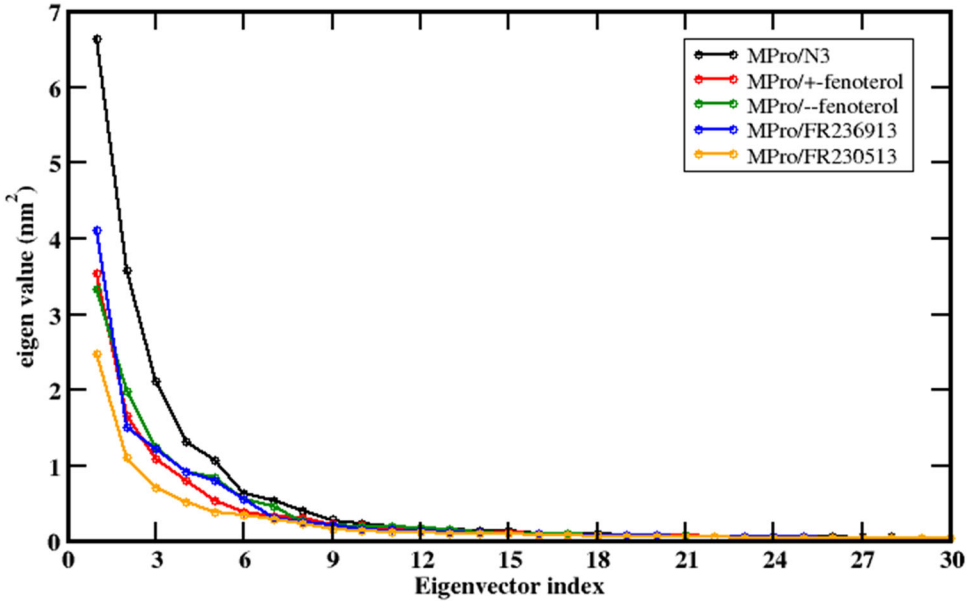


Figure 8. Plot of eigenvalue vs. first 30 eigenvector index derived from PCA over a stable trajectory of 40 ns for protein-ligand systems.

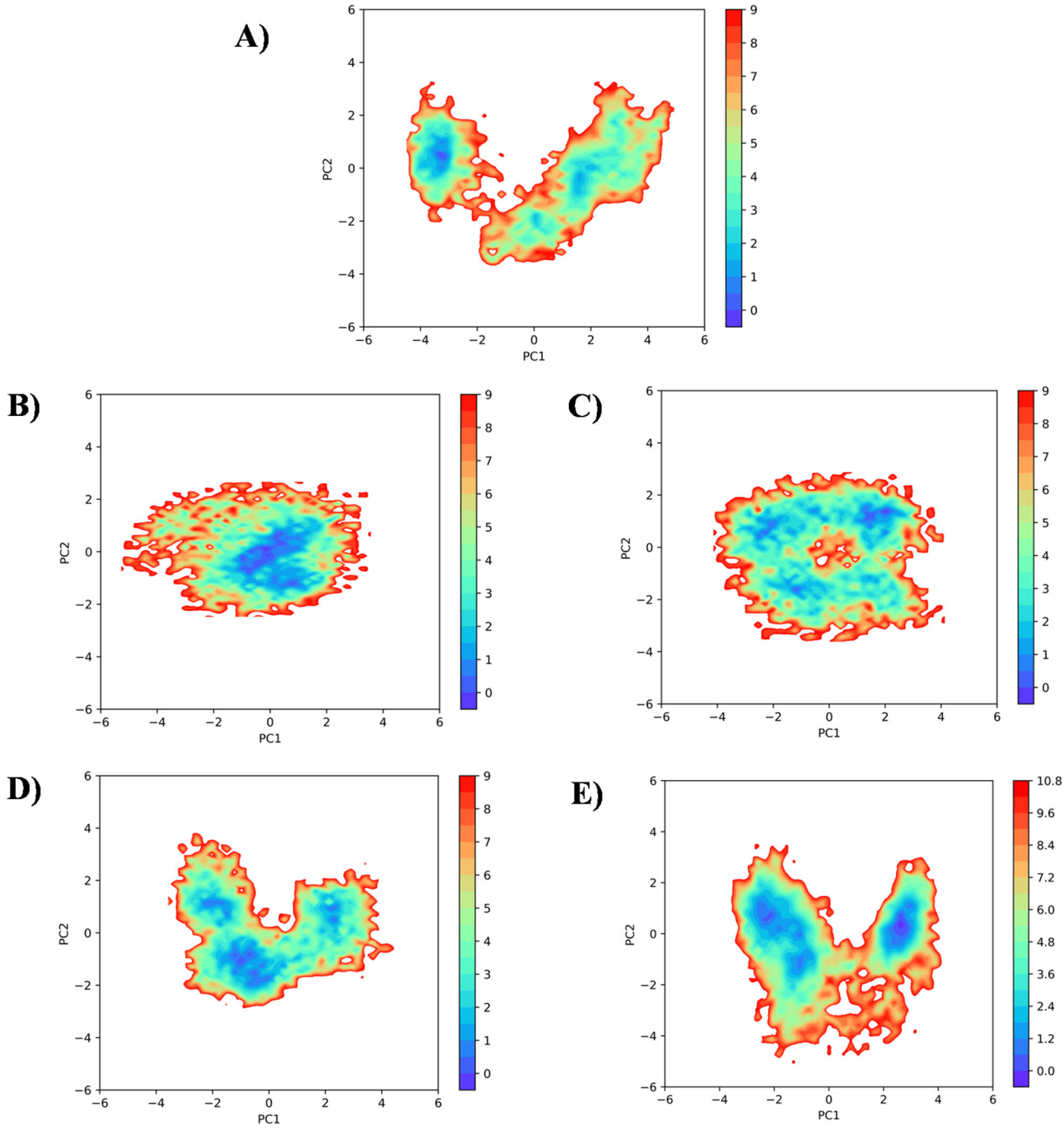


Figure 9. Free energy landscape from a stable 40 ns trajectory for all complexes using the reaction coordinates as the projection of backbone atoms of protease (6LU7) onto the first two principal components. (A) MPro/N3, (B) MPro/+-fenoterol, (C) MPro/−-fenoterol, (D) MPro/FR236913 and (E) MPro/FR230513.

Table 3. Contribution of energy components to MM/PBSA binding free energy for covid-19 main protease with potential hits (energy in kJ/mol).

| System | van der Waals energy | Electrostatic energy | Polar solvation energy | SASA | Binding energy |
|---|---|---|---|---|---|
| MPro (6LU7)/N3 | −254.015 ± 17.26 | −71.180 ± 13.29 | 209.180 ± 19.74 | −23.049 ± 1.16 | −138.788 ± 22.00 |
| MPro (6W63)/X77 | −206.926 ± 13.15 | −48.228 ± 14.91 | 174.388 ± 16.84 | −20.276 ± 1.00 | −101.042 ± 15.47 |
| MPro (6Y2G)/13b | −234.467 ± 22.70 | −102.426 ± 14.08 | 244.155 ± 21.88 | −23.763 ± 2.00 | −116.501 ± 17.85 |
| MPro (6LU7)/ +-fenoterol | −143.451 ± 14.53 | −262.777 ± 25.02 | 203.943 ± 25.09 | −15.501 ± 1.07 | −217.785 ± 14.99 |
| MPro (6LU7)/ −-fenoterol | −149.823 ± 12.09 | −233.150 ± 30.14 | 201.554 ± 28.10 | −15.933 ± 0.92 | −197.351 ± 14.80 |
| MPro (6LU7)/ FR236913 | −186.225 ± 19.09 | −42.974 ± 15.75 | 165.437 ± 27.34 | −18.687 ± 1.50 | −82.449 ± 15.91 |
| MPro (6LU7)/ FR230513 | −173.976 ± 9.75 | −39.467 ± 9.31 | 143.109 ± 9.45 | −16.449 ± 0.77 | −86.782 ± 10.54 |

## Conclusion

The present work describes the combined approach of ligand-based and structure-based virtual screening to obtain potential drug candidates as covid-19 main protease inhibitor. The drug-like molecules from ZINC database were screened and ranked based on docking score, fitness and Lipinski's rule of five. The molecular docking suggested 8

potential hits (4 each from adrenoceptor agonists and deaminase inhibitors) which showed lower binding energy with the protease. Out of 8, four molecules such as +/−-fenoterol, FR236913 and FR230513 were selected as top-scored hits. Docking suggested that hydrogen bond interactions with residues Gly143, Glu166 and Gln189 are crucial for ligand binding. The generated pharmacophore model contains three aromatic rings which indicate the possibility of stacking interactions with the residues. ADME/Toxicity prediction suggested that FR236913 has lower drug-likeness compared to other hit molecules. The stability of complex formed by four top-scored hits from the docking and co-crystal inhibitor N3 were analyzed by 100 ns MD simulation. The complexes of +/−-fenoterol, FR236913 and FR230513 were found to be stable than the native inhibitor N3, from RMSD, RMSF and Rg values. The complexes of adrenoceptor inhibitors (+/−-fenoterol) were stabilized by water-mediated hydrogen bonds with protein and ligand. PCA and FEL analysis suggests that flexibility of binding site residues helps the ligand to interact effectively with the enzyme. MM/PBSA calculations suggested that van der Waals energy and electrostatic energy are the crucial for the stability of complexes. The top-scored molecules predicted form molecular docking found to be an efficient inhibitor against main protease enzyme. The outcomes from this *in silico* study can be used to design and synthesize main protease inhibitors against novel coronavirus.

## Acknowledgment

We would like to thank Schrödinger Inc., Department of Chemistry and Department of Physics, NITK Surathkal for their constant support.

## Disclosure statement

Authors declare no conflict of interest.

## Funding

Funding from Department of Science and Technology, Science and Engineering Research Board, India (CRG/2019/000578) is highly acknowledged.

## ORCID

*Debashree Chakraborty* http://orcid.org/0000-0002-0142-7941

## References

Abraham, M. J., Murtola, T., Schulz, R., Páll, S., Smith, J. C., Hess, B., & Lindahl, E. (2015). GROMACS: High performance molecular simulations through multi-level parallelism from laptops to supercomputers. *SoftwareX*, *1-2*, 19–25. https://doi.org/10.1016/j.softx.2015.06.001

Ahmad, T., Khan, M., Haroon; Musa, T. H., Nasir, S., Hui, J., Bonilla-Aldana, D. K., & Rodriguez-Morales, A. J. (2020). COVID-19: Zoonotic aspects. *Travel Medicine and Infectious Disease*, *36*, 101607. https://doi.org/10.1016/j.tmaid.2020.101607

Baby, K., Maity, S., Mehta, C. H., Suresh, A., Nayak, U. Y., & Nayak, Y. (2020). Targeting SARS-CoV-2 main protease: A computational drug repurposing study. *Archives of Medical Research*, S0188440920309577. https://doi.org/10.1016/j.arcmed.2020.09.013

Barisione, G., Baroffio, M., Crimi, E., & Brusasco, V. (2010). Beta-adrenergic agonists. *Pharmaceuticals (Basel, Switzerland)*, *3*(4), 1016–1044. https://doi.org/10.3390/ph3041016

Bolelli, K., Ertan-Bolelli, T., Unsalan, O., & Altunayar-Unsalan, C. (2020). Altunayar-unsalan, C. fenoterol and dobutamine as COVID-19 main protease inhibitors: A virtual screening study. *Journal of Molecular Structure*, 129449. https://doi.org/10.1016/j.molstruc.2020.129449

Bussi, G., Donadio, D., & Parrinello, M. (2007). Canonical sampling through velocity rescaling. *The Journal of Chemical Physics*, *126*(1), 014101. https://doi.org/10.1063/1.2408420

Chojnacka, K., Witek-Krowiak, A., Skrzypczak, D., Mikula, K., & Młynarz, P. (2020). Phytochemicals containing biologically active polyphenols as an effective agent against Covid-19-inducing coronavirus. *The Journal of Functional Foods*, *73*, 104146. https://doi.org/10.1016/j.jff.2020.104146

Daddam, J. R., Sreenivasulu, B., Peddanna, K., & Umamahesh, K. (2020). Designing, docking and molecular dynamics simulation studies of novel cloperastine analogues as anti-allergic agents: Homology modeling and active site prediction for the human histamine H1 receptor. *RSC Advances*, *10*(8), 4745–4754. https://doi.org/10.1039/C9RA09245E

Das, B. K., Pv, P., & Chakraborty, D. (2019). Computational insights into factor affecting the potency of diaryl sulfone analogs as *Escherichia coli* dihydropteroate synthase inhibitors. *Computational Biology and Chemistry*, *78*, 37–52. https://doi.org/10.1016/j.compbiolchem.2018.11.005

Dixon, S. L., Smondyrev, A. M., Knoll, E. H., Rao, S. N., Shaw, D. E., & Friesner, R. A. (2006). PHASE: A new engine for pharmacophore perception, 3D QSAR model development, and 3D database screening: 1. Methodology and preliminary results. *Journal of Computer-Aided Molecular Design*, *20*(10-11), 647–671. https://doi.org/10.1007/s10822-006-9087-6

Fehr, A. R., & Perlman, S. (2015). Coronaviruses: An overview of their replication and pathogenesis. In Maier, H. J., Bickerton, E., & Britton, P. (Eds.), *Methods in molecular biology* (Vol. 1282, pp 1–23). New York: Springer. https://doi.org/10.1007/978-1-4939-2438-7_1

Glazer, R. I. (1980). Adenosine deaminase inhibitors: Their role in chemotherapy and immunosuppression. *Cancer Chemotherapy and Pharmacology*, *4*(4), 227-235. https://doi.org/10.1007/BF00255266

Gordon, D. E., Jang, G. M., Bouhaddou, M., Xu, J., Obernier, K., White, K. M., O'Meara, M. J., Rezelj, V. V., Guo, J. Z., Swaney, D. L., Tummino, T. A., Hüttenhain, R., Kaake, R. M., Richards, A. L., Tutuncuoglu, B., Foussard, H., Batra, J., Haas, K., Modak, M., … Krogan, N. J. (2020). A SARS-CoV-2 protein interaction map reveals targets for drug repurposing. *Nature*, *583*(7816), 459–468. https://doi.org/10.1038/s41586-020-2286-9

Gutierrez-Villagomez, J. M., Campos-García, T., Molina Torres, J., López, M. G., & Vázquez-Martínez, J. (2020). Alkamides and piperamides as potential antivirals against the Severe Acute Respiratory Syndrome Coronavirus 2 (SARS-CoV-2). *The Journal of Physical Chemistry Letters*, *11*(19), 8008–8016. acs.jpclett.0c01685. https://doi.org/10.1021/acs.jpclett.0c01685

Hornak, V., Abel, R., Okur, A., Strockbine, B., Roitberg, A., & Simmerling, C. (2006). Comparison of multiple amber force fields and development of improved protein backbone parameters. *Proteins*, *65*(3), 712–725. https://doi.org/10.1002/prot.21123

Irwin, J. J., Sterling, T., Mysinger, M. M., Bolstad, E. S., & Coleman, R. G. (2012). ZINC: A free tool to discover chemistry for biology. *Journal of Chemical Information and Modeling*, *52*(7), 1757–1768. https://doi.org/10.1021/ci3001277

Jin, Z., Du, X., Xu, Y., Deng, Y., Liu, M., Zhao, Y., Zhang, B., Li, X., Zhang, L., Peng, C., Duan, Y., Yu, J., Wang, L., Yang, K., Liu, F., Jiang, R., Yang, X., You, T., Liu, X., … Yang, H. (2020). Structure of Mpro from SARS-CoV-2 and discovery of its inhibitors. *Nature*, *582*(7811), 289–293. https://doi.org/10.1038/s41586-020-2223-y

Jorgensen, W. L., Maxwell, D. S., & Tirado-Rives, J. (1996). Development and testing of the OPLS all-atom force field on conformational energetics and properties of organic liquids. *Journal of the American*

*Chemical Society*, *118*(45), 11225–11236. https://doi.org/10.1021/ja9621760

Kaminski, G. A., Friesner, R. A., Tirado-Rives, J., & Jorgensen, W. L. (2001). Evaluation and reparametrization of the OPLS-AA force field for proteins via comparison with accurate quantum chemical calculations on peptides. *The Journal of Physical Chemistry B*, *105*(28), 6474–6487. https://doi.org/10.1021/jp003919d

Kumar, D., Kumari, K., Vishvakarma, V. K., Jayaraj, A., Kumar, D., Ramappa, V. K., Patel, R., Kumar, V., Dass, S. K., & Chandra, R. (2020). Promising inhibitors of main protease of novel corona virus to prevent the spread of COVID-19 using docking and molecular dynamics simulation. *Journal of Biomolecular Structure and Dynamics*, 1–15. https://doi.org/10.1080/07391102.2020.1779131

Kumar, Y., Singh, H., & Patel, C. N. (2020). In silico prediction of potential inhibitors for the main protease of SARS-CoV-2 using molecular docking and dynamics simulation based drug-repurposing. *Journal of Infection and Public Health*, *13*(9), 1210–1223. S1876034120305268. https://doi.org/10.1016/j.jiph.2020.06.016

Kumari, R., Kumar, R., & Lynn, A., Open Source Drug Discovery Consortium. (2014). g_mmpbsa-a GROMACS tool for high-throughput MM-PBSA calculations. *Journal of Chemical Information and Modeling*, *54*(7), 1951–1962. https://doi.org/10.1021/ci500020m

Li, S., & Hong, M. (2011). Protonation, tautomerization, and rotameric structure of histidine: A comprehensive study by magic-angle-spinning solid-state NMR. *Journal of the American Chemical Society*, *133*(5), 1534–1544. https://doi.org/10.1021/ja108943n

Lipinski, C. A. (2004). Lead- and drug-like compounds: The rule-of-five revolution. *Drug Discovery Today. Technologies*, *1*(4), 337–341. https://doi.org/10.1016/j.ddtec.2004.11.007

Mark, P., & Nilsson, L. (2001). Structure and dynamics of the TIP3P, SPC, and SPC/E water models at 298 K. *The Journal of Physical Chemistry A*, *105*(43), 9954–9960. https://doi.org/10.1021/jp003020w

Martyna, G. J., Klein, M. L., & Tuckerman, M. (1992). Nosé–Hoover Chains: The Canonical Ensemble via Continuous Dynamics. *The Journal of Chemical Physics*, *97*(4), 2635–2643. https://doi.org/10.1063/1.463940

Mittal, L., Kumari, A., Srivastava, M., Singh, M., & Asthana, S. (2020). Identification of potential molecules against COVID-19 main protease through structure-guided virtual screening approach. *Journal of Biomolecular Structure and Dynamics*, 1–19. https://doi.org/10.1080/07391102.2020.1768151.

Narkhede, R. R., Pise, A. V., Cheke, R. S., & Shinde, S. D. (2020). Recognition of natural products as potential inhibitors of COVID-19 Main Protease (Mpro): In-silico evidences. *Natural Products and Bioprospecting*, *10*(5), 297–306. https://doi.org/10.1007/s13659-020-00253-1

Parrinello, M., & Rahman, A. (1981). Polymorphic transitions in single crystals: A new molecular dynamics method. *Journal of Applied Physics*, *52*(12), 7182–7190. https://doi.org/10.1063/1.328693

Ren, X., Zeng, R., Wang, C., Zhang, M., Liang, C., Tang, Z., & Ren, J. (2017). Structural insight into inhibition of REV7 protein interaction revealed by docking, molecular dynamics and MM/PBSA studies. *RSC Advances*, *7*(44), 27780–27786. https://doi.org/10.1039/C7RA03716C

Riva, L., Yuan, S., Yin, X., Martin-Sancho, L., Matsunaga, N., Pache, L., Burgstaller-Muehlbacher, S., De Jesus, P. D., Teriete, P., Hull, M. V., Chang, M. W., Chan, J. F.-W., Cao, J., Poon, V. K.-M., Herbert, K. M., Cheng, K., Nguyen, T.-T H., Rubanov, A., Pu, Y., … Chanda, S. K. (2020). Discovery of SARS-CoV-2 antiviral drugs through large-scale compound repurposing. *Nature*, *586*(7827), 113–119. https://doi.org/10.1038/s41586-020-2577-1

Schoeman, D., & Fielding, B. C. (2019). Coronavirus envelope protein: Current knowledge. *Virology Journal*, *16*(1), 69. https://doi.org/10.1186/s12985-019-1182-0

Shah, B., Modi, P., & Sagar, S. R. (2020). In silico studies on therapeutic agents for COVID-19: Drug repurposing approach. *Life Sciences*, *252*, 117652. https://doi.org/10.1016/j.lfs.2020.117652

Svedmyr, N. (1985). Fenoterol: A beta2-adrenergic agonist for use in asthma. Pharmacology, pharmacokinetics, clinical efficacy and adverse effects. *Pharmacotherapy*, *5*(3), 109–126. https://doi.org/10.1002/j.1875-9114.1985.tb03409.x

Terasaka, T., Kinoshita, T., Kuno, M., & Nakanishi, I. (2004). A highly potent non-nucleoside adenosine deaminase inhibitor: efficient drug discovery by intentional lead hybridization. *Journal of the American Chemical Society*, *126*(1), 34–35. https://doi.org/10.1021/ja038606l

Terasaka, T., Kinoshita, T., Kuno, M., Seki, N., Tanaka, K., & Nakanishi, I. (2004). Structure-based design, synthesis, and structure-activity relationship studies of novel non-nucleoside adenosine deaminase inhibitors. *Journal of Medicinal Chemistry*, *47*(15), 3730–3743. https://doi.org/10.1021/jm0306374

Trincavelli, M. L. (2013). Unveiling the binding mode of adenosine deaminase inhibitors to the active site of the enzyme: Implication for rational drug design : Presented by Maria P. Abbracchio. *Purinergic Signalling*, *9*(1), 1–3. https://doi.org/10.1007/s11302-013-9353-8

Venugopal, P. P., Das, B. K., Soorya, E., & Chakraborty, D. (2020). Effect of hydrophobic and hydrogen bonding interactions on the potency of SS-alanine analogs of G-protein coupled glucagon receptor inhibitors. *Proteins: Structure, Function, and Bioinformatics*, *88*(2), 327–344. https://doi.org/10.1002/prot.25807

Wang, F., Chen, C., Tan, W., Yang, K., & Yang, H. (2016). Structure of main protease from human Coronavirus NL63: Insights for wide spectrum anti-Coronavirus drug design. *Scientific Reports*, *6*(1), 22677. https://doi.org/10.1038/srep22677

Wu, F., Zhao, S., Yu, B., Chen, Y.-M., Wang, W., Song, Z.-G., Hu, Y., Tao, Z.-W., Tian, J.-H., Pei, Y.-Y., Yuan, M.-L., Zhang, Y.-L., Dai, F.-H., Liu, Y., Wang, Q.-M., Zheng, J.-J., Xu, L., Holmes, E. C., & Zhang, Y.-Z. (2020). A new coronavirus associated with human respiratory disease in China. *Nature*, *579*(7798), 265–269. https://doi.org/10.1038/s41586-020-2008-3

Xue, X., Yu, H., Yang, H., Xue, F., Wu, Z., Shen, W., Li, J., Zhou, Z., Ding, Y., Zhao, Q., Zhang, X. C., Liao, M., Bartlam, M., & Rao, Z. (2008). Structures of two coronavirus main proteases: Implications for substrate binding and antiviral drug design. *Journal of Virology*, *82*(5), 2515–2527. https://doi.org/10.1128/JVI.02114-07

Yang, H., Yang, M., Ding, Y., Liu, Y., Lou, Z., Zhou, Z., Sun, L., Mo, L., Ye, S., Pang, H., Gao, G. F., Anand, K., Bartlam, M., Hilgenfeld, R., & Rao, Z. (2003). The crystal structures of severe acute respiratory syndrome virus main protease and its complex with an inhibitor. *Proceedings of the National Academy of Sciences of the United States of America*, *100*(23), 13190–13195. https://doi.org/10.1073/pnas.1835675100

Zhou, Y., Wang, F., Tang, J., Nussinov, R., & Cheng, F. (2020). Artificial intelligence in COVID-19 drug repurposing. *The Lancet Digital Health*, *2*(12), e667–e676. S2589750020301928. https://doi.org/10.1016/S2589-7500(20)30192-8